The spiking and secretory activity of oxytocin neurones in response to osmotic stimulation

The Journal of Physiology

https://jp.msubmit.net

JP-RP-2019-278045R1

Title: The spiking and secretory activity of oxytocin neurones in response to osmotic stimulation. A computational model.

Authors: Jorge Maicos-Royo
Gareth Leng
Duncan MacGregor

Author Conflict: No competing interests declared

Author Contribution: Jorge Maicos-Royo: Conception or design of the work; Acquisition or analysis or interpretation of data for the work; Drafting the work or revising it critically for important intellectual content; Final approval of the version to be published; Agreement to be accountable for all aspects of the work Gareth Leng: Conception or design of the work; Acquisition or analysis or interpretation of data for the work; Drafting the work or revising it critically for important intellectual content; Final approval of the version to be published; Agreement to be accountable for all aspects of the work Duncan MacGregor: Conception or design of the work; Drafting the work or revising it critically for important intellectual content; Final approval of the version to be published; Agreement to be accountable for all aspects of the work

Running Title: Oxytocin neurone computational model

Dual Publication: No

Funding: Seventh Framework Programme (EC Seventh Framework Programme): Gareth Leng, 607310

Title

The spiking and secretory activity of oxytocin neurones in response to osmotic stimulation. A computational model.

Running title.

Oxytocin neurone computational model

Keywords

posterior pituitary; lamina terminalis; osmotic pressure, hypovolemia; hypothalamus

Three key words

Oxytocin, computational, neuroendocrinology.

Contact information

duncan.macgregor@ed.ac.uk

Authors

Maícas Royo J, Leng G, MacGregor DJ

* Centre for Discovery Brain Sciences, The University of Edinburgh, Edinburgh, UK.

Author contributions.

The work is a computational work developed at the Centre for Discovery for Brain Sciences.

JMR, DM and GL contributed to the conception and design of the work.

JMR drafted the work and JMR, DM and GL revised it critically for important intellectual content.

JMR acquired and analysed the data. JMR, DM and GL interpreted the data.

Funding

This project received funding from the European Union's Seventh Framework Programme for research, technological development and demonstration under grant agreement n 607310.

Competing interests.

The authors have nothing to disclose.

Author profile

With an honours degree in engineering, another one in psychology and three masters, Jorge Maícas Royo spent his first ten professional years in the private sector, between IT companies and teaching informatics. In 2014, he began his PhD at the University of Edinburgh, where he developed a computational model for oxytocin neurones presented here in its latest version. Now, in a post doc position in Peter Kind's lab at the University of Edinburgh, he will be developing a computational model to capture rats' behavior without observer bias, in collaboration with Robert Datta at Harvard University.

Abstract

Magnocellular vasopressin and oxytocin neurones in the rat hypothalamus project to the posterior pituitary, where they secrete their products into the bloodstream. In rodents, both vasopressin and oxytocin magnocellular neurones are osmoresponsive, and their increased spiking activity is mainly a consequence of an increase synaptic input from osmoresponsive neurons in regions adjacent to the anterior wall of the third ventricle. Osmotically stimulated vasopressin secretion promotes antidiuresis while oxytocin secretion promotes natriuresis. In this work we tested a previously published computational model of the spiking and secretion activity of oxytocin cells against published evidence of changes in spiking activity and plasma oxytocin concentration in response to different osmotic challenges. We show that integrating this oxytocin model with a simple model of the osmoresponsive inputs to oxytocin cells achieves a strikingly close match to diverse sources of data. Comparing model predictions with published data using bicuculline to block inhibitory GABA inputs supports the conclusion that inhibitory inputs and excitatory inputs are co-activated by osmotic stimuli. Finally, we studied how the gain of osmotically stimulated oxytocin release changes in the presence of a hypovolemic stimulus, showing that this is best explained by an inhibition of an osmotically-regulated inhibitory drive to the magnocellular neurones.

Abbreviations

CCK cholecystokinin

EPSP excitatory post-synaptic potential

IPSP inhibitory post-synaptic potential

EVF extravascular fluid

ICF intracellular fluid

OVLT organum vasculosum of the lamina terminalis

Introduction

Magnocellular oxytocin neurones are large neurones in the hypothalamus that subserve a variety of important physiological functions. These neurones project to the posterior lobe of the pituitary and some also innervate diverse forebrain regions (Althammer & Grinevich 2017). At the pituitary, they secrete oxytocin into the systemic circulation, regulated by action potentials (spikes) propagated in their axons, and they can also release large amounts of oxytocin into the hypothalamus from their dendrites. Dendritic release is semi-independent of spike activity: it can be triggered by peptides that induce intracellular calcium release as well as by voltage-gated calcium entry triggered by spikes (Ludwig & Leng 2006).

Oxytocin secretion is essential for milk let-down in lactation and regulates parturition in mammals (Higuchi *et al.*, 1985; Russell & Leng, 1998). At term pregnancy (in response to signals from the contracting uterus) and in lactation (in response to the suckling of young) oxytocin cells discharge in quasi-synchronous bursts that lead to pulsatile secretion of oxytocin. The bursting arises from dendro-dendritic interactions involving oxytocin release, and occurs when dendritic stores of oxytocin have been primed to be available for spike-dependent release (see Rossoni *et al.* 2008 for references and a model of this reflex). In the absence of these specific stimuli, oxytocin cells fire independently and do not show intense bursting activity.

In rodents and in some other mammals (Rasmussen *et al.* 2003, 2004), oxytocin is also regulated by plasma osmotic pressure and blood volume to control sodium excretion at the kidneys (Verbalis *et al.* 1991; Gutkowska & Joankowski, 2009; Leng & Russell, 2018), and by a wide range of signals that regulate appetite and energy expenditure (Leng & Sabatier, 2017). In response to *these* stimuli, oxytocin cells fire continuously and proportionately, leading to sustained increases in plasma oxytocin concentration.

From electrophysiological studies *in vitro*, we now have a good understanding of the intrinsic properties of oxytocin neurones that underlie their spiking activity (e.g. Hatton & Li, 1999; Pittman *et al.* 1999; Armstrong *et al.* 2010; Brown *et al.* 2013; Armstrong *et al.* 2018). Spikes arise from perturbations in membrane potential evoked by excitatory and inhibitory post-synaptic potentials (EPSPs and IPSPs). When a spike is triggered, a hyperpolarising afterpotential (HAP) imposes a relative refractory period of typically about 30 ms. Spikes also evoke a small but long-lasting afterhyperpolarisation (AHP) that is the result of several Ca^{2+}-activated K^+ conductances. These spike-dependent changes in excitability account for

the spontaneous spiking patterns of most oxytocin cells *in vivo* (Richard *et al.* 1997; Leng *et al.* 1999; Hatton & Wang, 2008; Brown *et al.* 2013), as indicated by the excellent fit to recorded spike patterns that can be achieved with a Hodgkin-Huxley type model of the oxytocin cell stimulated by a randomly arriving mixture of EPSPs and IPSPs (Leng *et al.* 2017). This model in turn can be well approximated by a leaky integrate-and-fire neurone model adapted to include a simulated HAP and AHP (Maícas Royo *et al.* 2016).

The stimulus-secretion properties of the neurosecretory terminals have also been well characterised (Bicknell *et al.* 1984; Bicknell, 1988). Stimulus-secretion coupling is highly non-linear, but the features of this can also be modelled in a way that matches experimental data closely (MacGregor & Leng, 2013). Finally, the clearance of oxytocin from the blood has been extensively characterised (Ginsburg & Smith, 1959; Fabian *et al.* 1969; Leng & Sabatier, 2016).

Combining this understanding, we recently described a model linking oxytocin cell properties to spike activity, spike activity to secretion, and secretion to the dynamics of oxytocin in plasma (Maícas Royo *et al.* 2018). The model gives a close quantitative match to the behaviour of oxytocin cells in response to an appetite-related challenge (systemic injection of the gut hormone cholecystokinin, CCK) and to the ensuing changes in plasma oxytocin concentration. In that work, we used experimental data to fit the model. Here we *tested* this combined model. To do so we needed independent data comprising measurements of oxytocin neurone spiking activity and measurements of plasma oxytocin concentration.

An abundance of such data in the literature comes from studies of the osmotic responsiveness of oxytocin neurones. These neurones respond to increases in plasma osmotic pressure partly as a result of intrinsic osmosensitivity, but also as a result of increased afferent input arising directly and indirectly from osmoreceptors in other forebrain regions (Bourque, 2008; Zimmerman *et al.* 2017). Specifically, osmosensitive neurones in the subfornical organ and organum vasculosum of the lamina terminalis (OVLT) project directly to oxytocin (and vasopressin) cells of the supraoptic and paraventricular nuclei, and also indirectly via the nucleus medianus (Prager-Khoutorsky & Bourque, 2015; Choe *et al.* 2016). The osmotically regulated input involves an excitatory glutamatergic component, but also an inhibitory component, as osmotic stimuli result in increases in both GABA and glutamate release in the supraoptic nucleus as measured by microdialysis *in vivo* (Leng *et al.* 2001).

Using published data to test the combined model presented a fresh challenge. The experiments used a variety of experimental protocols: some measured activity and secretion in conditions of chronic challenge (Wakerley *et al.*, 1978; Verbalis *et al.*, 1986; Stricker *et al.*, 1987; Verbalis & Dohanics, 1991), others used an acute (Higuchi *et al.* 1988) or a slow intravenous Na^+ load (Leng *et al.* 2001), yet others used an acute i.p. injection of hypertonic NaCl (Brimble & Dyball, 1977). To use these data we first had to model the experimental challenges themselves. We did so by assuming that oxytocin cells increase their activity as a consequence of changes in $[Na^+]$ in the extracellular environment of osmoreceptive neurones, and that this results in an increase in EPSP and IPSP rate that is linearly proportional to $[Na^+]$. We therefore had to infer the dynamic profile of changes in local $[Na^+]$ arising in the different experimental circumstances from available data on plasma $[Na^+]$ and osmotic pressure. We neglected the intrinsic osmosensitivity of oxytocin cells (Bourque, 2008; Prager-Khoutorsky & Bourque, 2015), but this has no substantial consequence as, in the model, the effects of a depolarisation that is linearly proportional to osmotic pressure is similar to that of an increase in EPSP rate.

Given this model of the experimental challenges that have been used to study osmotic responses, we show here that the previously published model of the oxytocin system appears to be fully quantitatively predictive of the observed outcomes of those experiments. From spike activity, the changes in plasma oxytocin concentration can be reliably inferred and vice versa. We also show how the model can give predictive insight into features of physiological behaviour, in particular by revealing a likely mechanism by which hypovolemia alters the gain of osmoresponsiveness.

Methods

We used our previous models for the spiking (Maícas Royo *et al.* 2016), secretion, and plasma oxytocin dynamics (Maícas Royo *et al.* 2018). To these, we added a model to mimic how osmotic pressure changes following either intravenous (i.v.) or intraperitoneal (i.p.) NaCl injection or infusion, and to implement current understanding of how osmotic pressure is encoded by neural inputs to the oxytocin neurones (Figure 1). The models were developed using software written in C++ with a graphical interface based in the open-source wxWidgets library. The software simulates a population of oxytocin cells by running multiple threads in parallel, summing the secretory output of the cells to drive a single thread running the model

of plasma oxytocin concentration. Population simulations were run with 100 neurones for up to 10,000 s, using a 1-ms step size. A single run simulating 10,000s of activity of 100 neurones responding to a hyperosmotic infusion takes 60 s, running on a quad core Intel i7-2600K at 3.40 GHz processor.

Post synaptic potentials

In each model neurone, we model PSPs as exponentially decaying perturbations to the membrane voltage *V*, arriving at Poisson random intervals at mean rates I_{re} and I_{ri}. The time an EPSP arrives, e_{time} is defined by:

$$e_{time} = \frac{-\log(1 - N_{rand})}{I_{re}}$$

where N_{rand} is a random number between 0 and 1. IPSP arrival times, i_{time}, follow the same formula.

The osmotic model

In our model, both I_{re} and I_{ri} can be modified by changes in osmotic pressure. We simulated the effect of an injection or infusion of NaCl using a multi-compartment model, representing the amount of Na^+ in plasma (Na_p) and in the extravascular fluid (EVF, Na_{EVF}), the EVF volume ($Vol_{EVF(Na)}$) and the volume of intracellular fluid (ICF, Vol_{ICF}). Na^+ has a larger EVF volume of distribution than oxytocin ($Vol_{EVF(oxy)}$), but the plasma volume (Vol_p) is (obviously) the same for both oxytocin and Na^+. $Vol_{EVF(oxy)}$ is as calculated previously ((Maícas Royo *et al.* 2018) using data from Fabian *et al.* (1969). Depending on the [Na^+] gradient, Na^+ diffuses between plasma and the EVF. At the same time, water diffuses between the EVF and the ICF to maintain osmotic equilibrium, with consequent changes in the EVF and ICF volumes (Fig 1). Plasma volume is given a fixed value, dependent on body weight.

An injection or infusion of NaCl is modelled by setting its start time (t_{iv}) and duration (T_{NaCl}) and its quantity (k_{NaCl}) in mM, with infusion rate ($R_{i.v.} = k_{NaCl}.T_{NaCl}^{-1}$). The model distinguishes between i.v. and i.p. routes. For i.v. infusions, the compartment receiving the NaCl is the plasma, and Na^+ enters the EVF from plasma with time constant τ_{iv}. For i.p. injections, Na^+ enters the EVF, and diffuses into plasma with time constant τ_{ip}. Thus, for an i.v. injection:

$$\frac{dNa_p}{dt} = R_{iv} \cdot \delta_{iv} - \frac{G_d}{\tau_{iv}}$$

where $\delta_{iv} = 1$ if $t_{iv} \leq t \leq (t_{iv} + T_{NaCl})$ otherwise $\delta_{iv} = 0$.

The Na^+ diffusion gradient, G_d, is defined as:

$$G_d = [Na]_p - [Na]_{EVF}$$

where the concentration of Na^+ in plasma, $[Na]_p$, is:

$$[Na]_p = {Na_p}/{(Vol_P \cdot MW_{Na})}$$

MW_{Na} is the molar weight of Na^+, 22.9898 g mol^{-1}. The $[Na]_{EVF}$ follows a similar relationship:

$$[Na]_{EVF} = {Na_{EVF}}/{(Vol_{EVF(Na)} \cdot MW_{Na})}$$

Where Na_{EVF} varies as:

$$\frac{dNa_{EVF}}{dt} = \frac{G_d}{\tau_{iv}}$$

In the case of i.p. injection:

$$\frac{dNa_{EVF}}{dt} = R_{ip} \cdot \delta_{ip} - \frac{G_d}{\tau_{ip}}$$

where $\delta_{i.p.} = 1$ if $T_{ip} \leq t \leq T_{ip} + T_{NaCl}$, otherwise $\delta_{ip} = 0$ and:

$$\frac{dNa_p}{dt} = \frac{G_d}{\tau_{iv}}$$

The initial volumes for the plasma, EVF and ICF depend on the body weight of the rat, *B*, but not on its sex (Sheng & Huggins, 1979). Following Sheng & Huggins (1979), we fixed the total amount of body water as 60% of body weight. Of that, two thirds is in the ICF and the rest is in the EVF and plasma. In our previous work, we used a plasma volume, Vol_p, of 8.5 ml in 250-g rats (Maícas Royo *et al.* 2018), and we maintain that proportion here. Thus, initially:

$$Vol_{ICF} = 0.6 \cdot B \cdot 0.67$$

$$Vol_p = 8.5 \cdot \frac{B}{250}$$

$$Vol_{EVF(Na)} = (0.6 \cdot B \cdot 0.33) - Vol_p$$

In simulating an injection or infusion of NaCl, the plasma volume is assumed to remain constant (the volumes infused are small relative to the EVF volume), but EVF and ICF volumes change as $[Na^+]_{EVF}$ changes. These changes simulate the fast osmotic movement of water between the EVF and the ICF (Sidel & Solomon, 1957), with a time constant τ_{osmo} = 1.61 s^{-1}. The water movement follows the gradient, G_w, between the current $[Na^+]_{EVF}$ and the averaged $[Na^+]_{EVF}$ during the previous 2 s, $[Na^+]_{EVF\text{-}2s}$.

$$G_w = ([Na]_{EVF} - [Na]_{EVF-2s})$$

$$\frac{dVol_{EVF(Na)}}{dt} = \frac{G_w}{\tau_{osm}}$$

$$\frac{dVol_{ICF}}{dt} = -\frac{G_w}{\tau_{osm}}$$

Osmotic signal to the spiking model

An increase in extracellular $[Na^+]$ is sensed by neurones of the circumventricular organs. To simulate this, we added an input to the spiking model, assuming a linear relationship between the osmotically-dependent PSP rate I_{osmo}, and $[Na^+]_{EVF}$ (for i.v. infusions and injections) or $[Na^+]p$ (for i.p. injections).

$$I_{osmo} = \alpha \cdot ([Na^+] - \beta) \quad \text{for } [Na^+] > \beta \text{ and 0 otherwise}$$

The gradient (α) and threshold (β) were fitted to experimental data showing a linear increase in spike rate in response to increasing $[Na^+]$, as described below.

For EPSPs, the total rate I_{re} is the sum of the rate of osmoresponsive EPSPs (I_{osmo}) and the rate of osmotically-independent EPSPs ($I_{reBasal}$). The IPSP rate (I_{ri}) is a function of the EPSP rates:

$$I_{ri} = I_{ratioBasal} \cdot I_{reBasal} + I_{ratioOsmo} \cdot I_{osmo}$$

$I_{ratioBasal}$ and $I_{ratioOsmo}$ can be modified independently to separately affect osmotically-dependent or independent IPSPs, but take by default the same value, I_{ratio} = 0.75.

Spiking model

The rest of the model is as described previously (Maícas Royo *et al.* 2018). We fix the PSP magnitudes, e_h and i_h, at 2 mV, having opposite sign for EPSPs and IPSPs. At each 1-ms time step, the number of PSPs, e_n and i_n, arriving in each time step at random intervals e_{time} and i_{time}, are summed to give the input I:

$$I = (e_h . e_n + i_h . i_n)$$

V_{syn} represents the contribution of synaptic input to the oxytocin cell membrane voltage (*V*), and decays to 0 with time constant τ_{syn} corresponding to a half-life of 3.5 ms:

$$\frac{dV_{syn}}{dt} = -\frac{V_{syn}}{\tau_{syn}} + I$$

Initially, the model neurone is at resting potential, V_{rest} = -56 mV. If inputs raise the membrane potential *V* above a threshold V_{th} = -50 mV, the neurone produces a spike. This triggers a HAP and an AHP, and *V* evolves according to:

$$V = V_{rest} + V_{syn} - HAP - AHP$$

HAP has a fixed step amplitude (k_{HAP} = 30 mV) and a time constant (τ_{HAP}) that corresponds to a half-life of 7.5 ms, as in Maícas Royo *et al.* (2016, 2018). *AHP* has a much smaller amplitude (k_{AHP} = 1 mV) and τ_{AHP} is set to correspond to a much longer half-life of 350 ms, as previously:

$$\frac{dHAP}{dt} = -\frac{HAP}{\tau_{HAP}} + k_{HAP} \cdot \delta$$

$$\frac{dAHP}{dt} = -\frac{AHP}{\tau_{AHP}} + k_{AHP} \cdot \delta$$

where δ = 1 if a spike is fired at time *t*, and δ = 0 otherwise.

Secretion and plasma models

Previously (Maícas Royo *et al.* 2018) we modeled 250-g rats, and set a fixed Vol_p = 8.5 ml and a fixed $Vol_{EVF(oxy)}$ = 9.75 ml. Here, we defined these as a function of body weight (*B*) which varied from 190 to 400 g in the data we used:

$$Vol_p = 8.5 \cdot \frac{B}{250}$$

$$Vol_{EVF(oxy)} = 9.75 \cdot \frac{B}{250}$$

The other equations and parameter values are as in the previous work, for both the oxytocin secretion and clearance models.

Reference data

To fit the osmotic model, we used data from Leng *et al.* (2001) and Brimble & Dyball (1977). To connect the osmotic model with the oxytocin spiking model we used data from Leng *et al.* (2001) and Brimble & Dyball (1977). To test the coupling of the osmotic model, plus the oxytocin spiking model, with the oxytocin secretion and oxytocin plasma models we simulated experiments from Leng *et al.* (2001) and Higuchi *et al.* (1988). Finally, we simulated the effect of bicuculline and hypovolemia in oxytocin neurones under osmotic challenges, using data from Leng *et al.* (2001) and Stricker & Verbalis (1986).

Results

In our previous work (Maícas Royo *et al.* 2018) we developed a model that related the spiking activity of oxytocin cells to plasma oxytocin concentrations. Here we *tested* this model by assessing how well predictions of the model match experimental measurements. Both spiking activity and plasma oxytocin have been measured in studies of osmotically regulated secretion. To use as much of these data as possible, we needed to model the experimental challenges themselves.

We assumed that the rate of PSPs arriving at each oxytocin cell changes as a linear function of extracellular [Na^+]. The plasma [Na^+] is *not* directly the stimulus, because when hypertonic NaCl is infused slowly i.v., there is a rapid increment in plasma [Na^+] (Fig. 2A) that is not accompanied by a corresponding increment in spike activity; instead, spike activity and plasma [Na^+] increase slowly and linearly in parallel during continued infusion (Leng *et al.* 2001). The magnitude of the observed change in plasma [Na^+] during infusion implies a rapid transfer of Na^+ from plasma to EVF, so it appears to be changes in an extravascular compartment that are seen by the oxytocin cells and their inputs –presumably changes in the surrounding extracellular fluid (Fig. 1).

Multi-compartment model for Na^+ diffusion

As reported in Leng *et al.* (2001), a 30-min i.v. infusion of 2M NaCl at 0.26 µl min^{-1} produces a rise in plasma [Na^+] from 134.5 to 146 mM during the first 5 min, followed by a linear rise of 8.5 mM in the next 25 min. These experiments were on urethane-anaesthetized rats; urethane is a sodium salt, and the basal plasma [Na^+] was 134.5 mM and we assumed this to be the same in the EVF. The mean body weight of the rats was 350 g, corresponding to an initial EVF volume of 57.4 ml, a plasma volume of 11.9 ml and an ICF volume of 140.7

ml (see Methods). The data are closely fit (Fig. 2A) by assuming that plasma [Na^+] equilibriates with EVF with a time constant τ_{iv} of 0.0036 s^{-1}. After the infusion, plasma [Na^+] decreases to 144.7 mM over 10 min as it equilibriates with the EVF (Fig. 2A). $[Na^+]_{EVF}$ rises linearly throughout the infusion as Na^+ enters the EVF from plasma, accompanied by the transfer of 16.2 ml water from ICF (Fig. 2B), calculated as that required for equilibriation of osmotic pressure in all compartments.

We then modelled the i.p. injection of 1 ml 1.5M NaCl described in Brimble & Dyball (1977) who used urethane-anaesthetized rats of 300 g body weight. We assumed the same initial plasma [Na^+] as above (134.5 mM). [Na^+] was not measured in these experiments, but plasma osmotic pressure was, and we converted these measures to [Na^+] by subtracting 38.5 mOsmol (Fig 2D) to reflect other osmolytes in plasma and dividing the remainder by two. The plasma osmotic pressure data were fit by an inferred time constant of diffusion from EVF to plasma, τ_{ip}, of 0.0006 s^{-1} (Na^+ moves rapidly from plasma to EVF because plasma is under positive orthostatic pressure, but movement from EVF into plasma is much slower). In the model, $[Na^+]_{EVF}$ rises rapidly from 134.5 mM to 143 mM after the injection. It then quickly falls, equilibriating with plasma by 30 min (Fig. 2C), because of fast water flux from ICF to the EVF (8.8 ml in 3 s; Fig. 2E).

While NaCl is infused i.v., the plasma [Na^+] always exceeds the EVF [Na^+], and we used EVF [Na^+] as the input to the spiking model. However, when NaCl is injected i.p., the EVF [Na^+] in the peritoneum will initially greatly exceed the plasma [Na^+], and [Na^+] in the brain changes as Na^+ enters it from both blood and EVF. For i.p. injections, we assumed that the changes in brain extracellular [Na^+] are well approximated by plasma [Na^+] – i.e., that the brain extracellular [Na^+] equilibriates with the EVF [Na^+] at the same rate as plasma [Na^+] does.

Integration with the spiking and secretion model

The firing rate of oxytocin cells increases linearly during i.v. infusion of hypertonic NaCl, and we assumed that this arises from a linear relationship between extracellular [Na^+] and synaptic input rate. Here we used an oxytocin cell model with exactly the same intrinsic properties as defined previously (Maícas Royo *et al.* 2018), and set the basal PSP rate to match the observed basal firing rate. We also assumed that osmotic stimuli increase the rate of both EPSPs and IPSPs, as inferred by Leng *et al.* (2001). This left two free parameters: the slope of the relationship between PSP rate and extracellular [Na^+], and the ratio ($\underline{I_{ratio}}$) of

EPSPs and IPSPs in that signal. As detailed below, the response of oxytocin cells to i.v. NaCl could be well fit with I_{ratio} = 0.75 and with α, the slope of the relationship between plasma [Na+] and PSP rate, = 80. We kept these values for the rest of the simulations.

Figure 3 compares the response of the model to the response of a typical oxytocin cell (from Leng et al. 2001) to i.v. injection of 20 µg kg^{-1} CCK followed by i.v. infusion of 26 µl 2M NaCl (Fig. 3A). We adjusted the basal PSP rate to match the basal firing rate of 2.9 spikes s^{-1}. We simulated the CCK injection as in Maícas Royo *et al.* (2018), and the NaCl infusion as above, adjusting for a body weight of 350 g. The model response is very close to the observed responses to CCK and NaCl. Importantly, we made no attempt to *fit* the model to this cell except by setting the basal PSP rate; the comparison shown is the prediction from the generic oxytocin cell model described in Leng *et al.* (2017). In the simulation, the firing rate responds to the NaCl infusion with an increase in firing rate from 2.3 spikes s^{-1} (Fig 3B left) to 10.5 spikes s^{-1} (Fig 3B right). At the basal rate, the model predicts an average secretion rate of 0.13 fg s^{-1}, and second-by second secretion rates fluctuate between 0 and 1 fg s^{-1} (Fig 3C left). After the infusion, the predicted mean secretion rate is 9.75 fg s^{-1}, 77 times more than during basal activity, fluctuating between 5.5 and 16.7 fg s^{-1} (Fig. 3C right). The predicted secretion rates fluctuate much more than the spike rate because of the non-linearity of stimulus-secretion coupling.

Responses to i.v. infusions of NaCl

Oxytocin cells are heterogeneous in their basal firing rates. Here, we incorporated this heterogeneity by varying the basal PSP rate using a lognormal distribution to match the mean and SD of experimental data. We simulated populations of cells to mimic the numbers of cells recorded in experiments and their variation in basal firing rate, and to fit the measured basal oxytocin plasma concentration.

We started by mimicking the response of 12 oxytocin cells to a 60-min i.v. infusion of 2M NaCl at 26 µl min^{-1} as in Leng *et al.* (2001). We simulated a 350-g rat, setting a mean (SD) PSP rate of 305(150) s^{-1} to obtain a basal firing rate of 3.1 spikes s^{-1}, matching the reported basal rate. The model showed a linear increase in the mean firing rate, matching the experimental data very closely (Fig 4A).

Leng *et al* (2001) also measured plasma oxytocin during similar infusions, but in different experimental conditions: these rats were also anaesthetized with urethane, but the transpharyngeal surgery involved in recording was not performed. In these conditions, basal

oxytocin concentrations are lower, apparently because the stress of surgery elevates basal neuronal activity. Accordingly, it was necessary to estimate the basal firing rate from the plasma concentration at rest.

We used plasma oxytocin data from Leng *et al*. (2001). To match the basal oxytocin concentration, we set the mean PSP rate at 190 s^{-1} in a population of 100 model neurones, randomizing lognormally the PSP rate from neuron to neuron to give a SD of 95 s^{-1}.That gave a mean (SD) firing rate of 1.4 (0.6) spikes s^{-1} and a plasma oxytocin concentration of 15.7 pg ml^{-1} (Fig. 4B). With the predicted induced increment in $[Na^+]$ of 20.2 mOsm, the model predicts oxytocin concentrations very close to observed levels.

Responses to i.p. injections of NaCl

Brimble & Dyball (1977) recorded 11 oxytocin cells in 300-g rats, and i.p. injection of 1 ml 1.5M NaCl increased their mean spike activity from 1.8 to 6.6 spikes.s^{-1} in the 12 min after the injection (Fig. 4C). We simulated this for a 300-g rat and 30 model neurones with a mean (SD) basal firing rate of 1.8 (0.4) spikes.s^{-1}, obtained by a lognormally randomized PSP mean (SD) rate of 215 (100) s^{-1} (Fig 4C). The predicted change in firing rate is again very close to the experimental data.

Responses to i.v. injection of NaCl

We matched the plasma oxytocin response after i.v. injection of 0.38 ml 1.5M NaCl in 190-g rats reported by Higuchi *et al.* (1988). In these experiments, the basal oxytocin concentration was mimicked in a population of 100 model neurons with a PSP rate of 132 (65) s^{-1}, producing a mean firing rate of 0.75(0.8) spikes.s^{-1}, associated with a plasma concentration of 10.6 pg.ml^{-1}. We simulated the i.v. injection, obtaining a close match (Fig 4D).

The relationship between firing rate and osmotic pressure

Brimble & Dyball (1977) showed the recorded firing rates of 50 oxytocin cells from rats with different osmotic pressures following i.p. injections of hypertonic saline or intragastric water loading. To construct the relationship of mean firing rate to osmotic pressure, we made 50 runs of 60 min of the model for a single neuron. Every run had a basal PSP rate of I_{re} = 170(85) s^{-1}, and in each run the value of $[Na^+]$ was raised by 0.5 mOsmol kg^{-1}, from 127 to 151.5 mOsmol kg^{-1} (to match the reported change in osmolality). The model prediction matches the experimental data closely (Fig 4E). The model data are also consistent with data reported by Negoro *et al.* (1987); they reported a mean firing rate of 1.7 ± 0.6 spikes.s^{-1} for 23 oxytocin cells in rats with a mean osmotic pressure of 299 ± 2.4 mOsmol.kg^{-1}; their

activity increased to 4.6 ± 0.6 spikes.s^{-1} after an i.p. injection of hypertonic NaCl that raised osmotic pressure to 313 ± 2.4 mOsmol.kg^{-1}.

The role of IPSPs in the osmotic response

We used the combined model to simulate the effect of blocking GABA receptors with bicuculline, delivered to the dendritic zone of the supraoptic nucleus, as described in Leng *et al.* (2001). In that work, five oxytocin cells were challenged with two 10-min infusions of 2M NaCl i.v. at 26 µl.min^{-1} before and after bicuculline. Bicuculline enhanced the neuronal response to osmotic pressure, implying that GABA inputs modulate the gain of the response (Fig 5A). We simulated that experiment by running our model with two populations of 20 neurones with a PSP rate of I_{re} = 210 (100) s^{-1}, and mimicked the effect of bicuculline by making I_{ri} = 0 in one of the populations. After 10-min infusion, the difference in firing rate increment between the populations was ~1.5 spikes.s^{-1}, very close to that observed experimentally (Fig 5B).

The osmotic response in hypovolemic rats

Using polyethylene glycol to reduce the plasma volume by 35-40%, Stricker & Verbalis (1986) and Stricker *et al.* (1987) found a steeper relationship between plasma oxytocin concentration and osmotic pressure (Fig 6A). Our model is fitted to plasma oxytocin concentrations measured with the Higuchi radioimmunoassay (Higuchi *et al.*, 1985), but these studies used a different radioimmunoassay (Amico *et al.* 1985), which consistently reported lower plasma oxytocin concentrations. Therefore, here we compared proportional changes not absolute values, which in the model are ~20 times higher than in the experimental data (see Discussion).

To simulate hypovolemia, we set the IPSP rate I_{ri} = 0 (Fig 6B). This produces a steeper relationship between secretion and [Na^+], but the rate of secretion saturates in a way that seemed inconsistent with experimental data. However, we found a better match by both reducing IPSPs while reducing the plasma volume by 35% while increasing the EVF volume by the same amount lost by the plasma, i.e. by simulating the shift in body water between compartments produced by polyethylene glycol (Fig. 6C). This implies that, after polyethylene glycol, the reduction in plasma volume together with the corresponding increment in EVF is responsible for a substantial part of the higher plasma oxytocin concentrations *independently of any change in secretion rate*.

Discussion

Oxytocin is not involved in fluid balance in humans (Rasmussen *et al.*, 2003, 2004), but in rodents oxytocin cells respond as strongly as vasopressin cells to osmotic challenges as measured either by their electrophysiological responses, or by measures of secretion (Leng and Russell, 2018). Here, we used our oxytocin spiking, secretion and oxytocin plasma clearance model to simulate the response of oxytocin cells to hyperosmotic challenges.

Oxytocin cells in the rat respond strongly to changes in plasma osmotic pressure from studies of electrical activity, gene expression and hormone secretion, and we understand at least some of the mechanisms involved (Bourque, 2008; Leng & Russell, 2018). Modelling in this case is a test of the *coherence* and *completeness* of our understanding. If our understanding of the intrinsic properties of oxytocin cells, of stimulus-secretion mechanisms, and of the dynamics of oxytocin clearance is good, then we should be able to translate that understanding into a computational model that quantitatively matches experimental data.

However, there is a problem. The conclusions that oxytocin cells are activated by osmotic stimuli and that oxytocin secretion is increased have been extensively replicated, so there is an abundance of experimental data. But these are *conceptual* replications, not exact experimental replications – and quantitatively exact experimental replications are practically inconceivable because they inevitably involve *some* differences in experimental conditions or methodologies. So *either* models must be fit to a biased selection of the data and are thus validated only for those particular experimental conditions, *or* an attempt must be made to incorporate as much experimental data as possible. The latter path involves modeling the experimental conditions themselves, including those differences that are likely to give rise to quantitative differences in outcomes.

To use data from different routes of administration of NaCl, we had to model the dynamics of $[Na^+]$ in the rat body. To do so, we adapted the two-compartment model for the oxytocin clearance implemented in our previous work by adding a third compartment, the ICF, which maintains osmotic equilibrium with the EVF by exchange of water. Once this model was developed, we coupled it to our previous model for oxytocin cells. This study was conceived as a *test* of our published model, so we changed only parameters necessary to simulate the experimental conditions, with one exception. In our previous work we set I_{ratio}, (the ratio between the EPSPs and the IPSPs) equal to 1. This was an arbitrary choice as nothing in the data determined it, nor did it have any implications for the fits in that study. Here, we set I_{ratio}

= 0.75 which gives a linear relationship between PSP rate (I_{re}) and firing rate and fits the bicuculline data well (Fig 5B); the relationship between I_{re} and firing rate becomes non-linear with a larger I_{ratio} (in cell models with an AHP) while a smaller I_{ratio} worsens the fit to the bicuculline data. This argument assumes that the relationship between PSP rate and osmotic pressure is approximately linear above a threshold; we have no direct evidence for this, it can be defended only by experimental evidence that the intrinsic properties of osmosensitive neurones in the circumventricular organs are similar to those of oxytocin cells, together with the evidence that oxytocin cells respond linearly to changes in osmotic pressure.

Alternative ways to ensure linearity between PSP rate and firing rate would be to use a smaller AHP or to add a depolarising afterpotential, as is needed to model at least some oxytocin cells (Maícas Royo *et al.*, 2016). In reality, oxytocin cells are heterogeneous with differing intrinsic properties and differing synaptic inputs, and we have not attempted to model this full heterogeneity. Again we must reflect on this: electrophysiological data come from single cells; we can average these data to estimate average population characteristics, and build a single cell model that reflects those. But a model of the "average" cell will not necessarily be the same as the average of individually modelled cells. Obviously we would like this to be true, and some confidence that it holds reasonably true in this case comes from the close matches that we obtained to diverse experimental data.

When fitting the model, we tried to use as much as possible of the electrophysiological data that we could find in the literature. Generally, electrophysiological data from *in vivo* experiments seemed reasonably consistent between experiments, but we had to make some choices. For instance, like the data in Fig. 5E from Brimble & Dyball (1977), the findings from Wakerley *et al.* (1978) indicate a linear relationship between osmotic pressure and spike rate, but with a smaller slope. The latter data are from yet another way of altering osmotic pressure – with chronic dehydration. In this case there is likely to be a more certain match between plasma [Na^+] and EVF [Na^+], which should be in equilibrium in these conditions, but we can expect some adaptation of cell properties with chronic osmotic stimulation, so we did not use the data from Wakerley *et al.* (1978).

Choosing studies of plasma oxytocin presented a greater problem. Measurements of plasma oxytocin differ according to the assay used, and one source of this variability arises from interference of the plasma matrix with immunoassays (Leng & Sabatier, 2016). Specifically, problems arise when large molecules in plasma interfere with the antibody, occluding the antigen recognition site and giving inflated values as a consequence. If the level of

interference is low, the consequence is a linearly proportionate exaggeration of true values in plasma; if interference is high there is an additional issue of a high and wholly erroneous baseline. The extent of this problem varies considerably with different antibodies, and with most antibodies the problem is so great that extraction of plasma samples to eliminate large molecules is strictly essential. Here, as in our previous work (Maícas Royo *et al.* 2018), we matched the model to experimental data that used the Higuchi immunoassay (Higuchi *et al.* 1985). This assay was apparently well validated for use on *unextracted* rat plasma, and has been particularly useful as it allowed smaller blood samples to be taken, facilitating studies with multiple sequential samples. Using this assay in our own studies we (G Leng, unpublished) confirmed that plasma levels of oxytocin from hypophysectomised rats were undetectable with this assay. However, the absolute values measured in intact rats are generally higher than in other assays using extraction – and such a discrepancy is apparent in Fig. 4A. This suggests that a low level of plasma matrix interference inflates plasma measurements using the Higuchi assay. As stocks of the Higuchi antibody are now exhausted further investigations with it are impossible.

Thus, the *absolute* levels of oxytocin predicted by this model are contestible, but as we understand the likely nature of the discrepancies, they affect only the scaling of oxytocin concentrations. Comparing values of oxytocin measured in studies that use the Higuchi assay with similar studies using radioimmunoassays on extracted samples suggests that values with the Higuchi assay are typically about 5 fold higher. For example, Brimble et al. (1978) reported that an i.p. injection of 1 ml 1.5M NaCl which raised the plasma osmotic pressure of urethane anesthetised lactating rats by 12 1 mOsmole.kg^{-1} increased the mean plasma concentration of oxytocin from 4.6 ± 0.7 pg.ml^{-1} to 24 ± 6 pg.ml^{-1} after 30 min, as measured by a radioimmunoassay on extracted plasma. Blackburn *et al.* (1987) using the Higuchi assay in urethane-anaesthetized virgin female rats reported basal levels of 28 5 pg.ml^{-1} rising to 118 ± 10 pg.ml^{-1} after 30 min after a similar injection. However there is a bigger discrepancy with studies using the Pittsburgh Ab-2oxytocin antiserum of Amico *et al.* (1985); these have consistently reported plasma concentrations lower than found with any other antiserum. For example, Bononi *et al.* (1993) reported basal concentrations of ~1 pg ml^{-1} in normonatraemic lactating rats rising by at most 10 pg ml^{-1} in response to suckling; as 1-2 ng is released into the circulation at each reflex milk ejection (Wakerley et al. 1973) these are much lower than would be expected. Thus the present model can be considered quantitatively consistent with

experimental measurements of oxytocin using the Higuchi assay, but absolute values in the model should be rescaled for any comparisons with data using different assays.

There are other problems; the model relates oxytocin activity to [Na^+], but many studies measure osmotic pressure not [Na^+]. Plasma measurements of osmotic pressure vary according to the method used, apparently because different methods variably detect contributions from colloid and other plasma constituents. Accordingly conversion from osmotic pressure to [Na^+] involves uncertainties, mainly affecting basal levels rather than relative changes.

The current model implements the assumption that both i.v. and i.p. injections of hypertonic NaCl selectively activate osmoresponsive synaptic inputs. However, in male rats (Shibuki *et al*. 1988). i.p. injections of hypertonic NaCl induce a transient increase in the activity of continuously firing supraoptic neurones that precedes the sustained rise that accompanied osmotic pressure changes. This transient response, which probably arises from activation of nociceptive afferents, was absent in the results of Brimble and Dyball (1977) that we modelled here. The difference may arise either from the fact that Brimble and Dyball's experiments were in lactating rats, which are known to be hyporesponsive to stressors (Slattery & Neumann 2008), or from the fact that their data were exclusively from identified oxytocin neurones. The later, sustained change in spike rate is, however, very similar in the two sets of data.

Finally, a major motivation in modeling the oxytocin system was to reconcile the linearity of oxytocin cell responses to hypertonic saline infusion with the intrinsic non linearities of oxytocin neuronal properties, and with the non-linearity of oxytocin secretion in response to the infusions. This led us to question of how a change in the apparent slope of the oxytocin response to osmotic pressure change can arises in hypovolemic conditions. We recognized that this can in part be explained by inferring that hypovolemia selectively inhibits an osmotically regulated inhibitory input to the oxytocin cells, but we recognized that this cannot be the full explanation. We noted though a point that has hitherto apparently gone unnoticed – that hypovolemia can raise measured plasma hormone measurements even if there is no change at all in the rate of secretion. This arises when hypovolemia is induced by polyethylene glycol injections as a consequence of the resultant shift in body water into the EVF from plasma and ICF. With a reduced plasma volume, a given rate of secretion produces a higher oxytocin concentration in plasma. With an expanded EVF there is increased entry of oxytocin from plasma into EVF. As oxytocin is cleared only from the plasma and not from

EVF, the total body content of oxytocin must therefore increase. In a steady state, the concentrations of oxytocin equalize in plasma and EVF, but at an elevated level. As the model shows, this is not a minor effect, but can explain a substantial part of the rise in plasma oxytocin concentration observed experimentally.

Acknowledgements.

This work was supported by the European Union's Seventh Framework Programme for Research, Technological Development, and Demonstration under Grant n 607310.

References

Althammer F & Grinevich V (2017). Diversity of oxytocin neurons: beyond magno- and parvocellular cell types? *J Neuroendocrinol*. doi: 10.1111/jne.12549.

Amico JA, Ervin MG, Leake RD, Fisher DA, Finn FM & Robinson AG (1985). A novel oxytocin-like and vasotocin-like peptide in human plasma after administration of estrogen. *J Clin Endocrinol Metab* 60, 5–12.

Armstrong WE, Wang L., Li C & Teruyama R (2010). Performance, properties and plasticity of identified oxytocin and vasopressin neurones in vitro. *J Neuroendocrinol* 22, 330–342.

Armstrong WE, Foehring RC, Kirchner MK & Sladek CD (2018). Electrophysiological Properties of Identified Oxytocin and Vasopressin Neurons. *J Neuroendocrinol.* e12666. doi: 10.1111/jne.12666

Bicknell RJ (1988). Optimizing release from peptide hormone secretory nerve terminals. *J Exp Biol* 139, 51–65.

Bicknell RJ, Brown D, Chapman C, Hancock PD & Leng G (1984). Reversible fatigue of stimulus-secretion coupling in the rat neurohypophysis. *J Physiol* 348, 601–613.

Blackburn RE, Leng G & Russell JA (1987). Control of magnocellular oxytocin neurones by the region anterior and ventral to the third ventricle (AV3V region) in rats. *J Endocrinol.* 114, 253-261.

Bononi PL, Janosky JE, Amico JA (1993). The oxytocin secretory response during suckling in the hypoosmolar lactating rat. *Brain Res*. 617:50-54.

Bourque CW (2008). Central mechanisms of osmosensation and systemic osmoregulation. *Nat Rev Neurosci* 9, 519–531.

Brimble MJ & Dyball REJ (1977). Characterization of the responses of oxytocin- and vasopressin-secreting neurones in the supraoptic nucleus to osmotic stimulation. *J Physiol* 271, 253–271.

Brimble MJ, Dyball RE & Forsling ML (1978). Oxytocin release following osmotic activation of oxytocin neurones in the paraventricular and supraoptic nuclei. *J Physiol.* **278**, 69-78.

Brown CH, Bains JS, Ludwig M & Stern JE (2013). Physiological regulation of magnocellular neurosecretory cell activity: Integration of intrinsic, local and afferent mechanisms. *J Neuroendocrinol*; DOI: 10.1111/jne.12051.

Choe KY, Trudel E & Bourque CW (2016). Effects of salt loading on the regulation of rat hypothalamic magnocellular neurosecretory cells by ionotropic GABA and glycine receptors. *J Neuroendocrinol*; DOI: 10.1111/jne.12372.

Fabian M, Forsling ML, Jones JJ & Lee J (1969). The release, clearance and plasma protein binding of oxytocin in the anaesthetized rat. *J Endocrinol* **43,** 175–189.

Ginsburg M & Smith MW (1959). The fate of oxytocin in male and female rats. *Br J Pharmacol Chemother* **14,** 327–333.

Gutkowska J, Jankowski M (2009). Oxytocin: old hormone, new drug. *Pharmaceuticals (Basel).* **2**, 168-183

Hatton G & Wang Y (2008). Neural mechanisms underlying the milk ejection burst and reflex. In *Progress in Brain Research*, pp. 155–166. Elsevier.

Hatton GI & Li Z –H. (1999). Neurophysiology of magnocellular neuroendocrine cells: Recent advances. *Prog Brain Res* **119,** 77–99.

Higuchi T, Honda K, Fukuoka T, Negoro H & Wakabayashi K (1985). Release of oxytocin during suckling and parturition in the rat. *J Endocrinol* **105,** 339–346.

Higuchi T, Honda K, Takano S & Negoro H (1988). Reduced oxytocin response to osmotic stimulus and immobilization stress in lactating rats. *J Endocrinol* **116,** 225–230.

Järvelä K, Koskinen M & Kööbi T (2003). Effects of hypertonic saline (7.5%) on extracellular fluid volumes in healthy volunteers. *Anaesthesia* **58,** 878–881.

Leng G, Brown CH, Bull PM, Brown D, Scullion S, Currie J, Blackburn-Munro RE, Feng J, Onaka T, Verbalis JG, Russell JA & Ludwig M (2001). Responses of magnocellular neurons to osmotic stimulation involves coactivation of excitatory and inhibitory input: an experimental and theoretical analysis. *J Neurosci* **21,** 6967–6977.

Leng G, Brown CH & Russell JA (1999). Physiological pathways regulating the activity of magnocellular neurosecretory cells. *Prog Neurobiol* **57,** 625–655.

Leng G & Sabatier N (2016). Measuring oxytocin and vasopressin: bioassays, immunoassays and random numbers. *J Neuroendocrinol* **28**(10). doi: 10.1111/jne.12413.

Leng G & Sabatier N (2017). Oxytocin – The sweet hormone? *Trends Endocrinol Metab* **28,** 365–376.

Leng T, Leng G & MacGregor DJ (2017). Spike patterning in oxytocin neurons: Capturing physiological behaviour with Hodgkin-Huxley and integrate-and-fire models. *PLOS ONE* **12,** e0180368.

Leng G & Russell JA (2018). The osmoresponsiveness of oxytocin and vasopressin neurones: mechanisms, allostasis and evolution. *J Neuroendocrinol.* Nov 19:e12662.

Ludwig M & Leng G (2006). Dendritic peptide release and peptide-dependent behaviours. *Nat Rev Neurosci* **7,** 126–136.

MacGregor DJ & Leng G (2013). Spike triggered hormone secretion in vasopressin cells; a model investigation of mechanism and heterogeneous population function. *PLoS Comput Biol* **9,** e1003187.

Maícas Royo J, Brown CH, Leng G & MacGregor DJ (2016). Oxytocin neurones: intrinsic mechanisms governing the regularity of spiking activity. *J Neuroendocrinol* **28,**(4). doi: 10.1111/jne.12358.

Maícas Royo J, Leng G & MacGregor DJ (2018). A predictive, quantitative model of Spiking activity and stimulus-secretion coupling in oxytocin neurons. *Endocrinology* **159,** 1433–1452.

Mazzoni MC, Borgstrom P, Arfors K-E & Intaglietta M (1988). Dynamic fluid redistribution in hyperosmotic resuscitation of hypovolemic hemorrhage. *Am J Physiol* **255,** H629–H637.

Negoro H, Honda K, Uchide K & Higuchi T (1987). Facilitation of milk ejection-related activation of oxytocin-secreting neurones by osmotic stimulation in the rat. *Brain Res.*

Pittman Q, Kombian SB, Mouginot D, Chen X & van Eerdenberg FJCM (1999). Electrophysiological studies of neurohypophysial neurons and peptides. *Prog Brain Res* **119,** 311–320.

Prager-Khoutorsky M & Bourque CW (2015). Mechanical basis of osmosensory transduction in magnocellular neurosecretory neurones of the rat supraoptic Nucleus. *J Neuroendocrinol* **27,** 507–515.

Rasmussen MS, Simonsen JA, Sandgaard NCF, Høilund-Carlsen PF & Bie P (2003). Mechanisms of acute natriuresis in normal humans on low sodium diet. *J Physiol* **546,** 591–603.

Rasmussen MS, Simonsen JA, Sandgaard NCF, Høilund-Carlsen PF & Bie P (2004). Effects of oxytocin in normal man during low and high sodium diets. *Acta Physiol Scand* **181,** 247–257.

Richard P, Moos F, Dayanithi G, Gouzènes L & Sabatier N (1997). Rhythmic activities of hypothalamic magnocellular neurons: Autocontrol mechanisms. *Biol Cell* **89,** 555–560.

Rossoni E, Feng J, Tirozzi B, Brown D, Leng G & Moos F (2008). Emergent synchronous bursting of oxytocin neuronal network. *PLOS Comput Biol* **4,** e1000123.

Russell JA & Leng G (1998). Sex, parturition and motherhood without oxytocin? *J Endocrinol* **157,** 343–359.

Sheng H-P & Huggins RA (1979). A review of body composition studies with emphasis on total body water and fat. *Am J Clin Nutr* **32,** 630–647.

Shibuki K, Leng G & Way S (1985). Effects of naloxone and of intraperitoneal hypertonic saline upon oxytocin release and upon supraoptic neuronal activity. *Neurosci Lett* **88,** 75-80.

Sidel VW & Solomon AK (1957). Entrance of water into human red cells under an osmotic pressure gradient. *J Gen Physiol* **41,** 243–257.

Slattery DA & Neumann ID (2008). No stress please! Mechanisms of stress hyporesponsivenes of the maternal brain. *J Physiol* **586,** 377-385.

Stricker EM, Hosutt JA & Verbalis JG (1987). Neurohypophyseal secretion in hypovolemic rats: inverse relation to sodium appetite. *Am J Physiol-Regul Integr Comp Physiol* **252,** R889–R896.

Stricker EM & Verbalis JG (1986). Interaction of osmotic and volume stimuli in regulation of neurohypophyseal secretion in rats. *Am J Physiol-Regul Integr Comp Physiol* **250,** R267–R275.

Verbalis JG, Baldwin EF & Robinson AG (1986). Osmotic regulation of plasma vasopressin and oxytocin after sustained hyponatremia. *Am J Physiol* **250,** R444-451.

Verbalis JG & Dohanics J (1991). Vasopressin and oxytocin secretion in chronically hyposmolar rats. *Am J Physiol* **261,** R1028-1038.

Verbalis JG, Mangione MP & Stricker EM (1991). Oxytocin produces natriuresis in rats at physiological plasma concentrations. *Endocrinology* **128**, 1317-1322.

Wakerley JB, Dyball RE & Lincoln DW (1973). Milk ejection in the rat: the result of a selective release of oxytocin. *J Endocrinol.* 57:557-558.

Wakerley JB, Poulain DA & Brown D (1978). Comparison of firing patterns in oxytocin- and vasopressin-releasing neurones during progressive dehydration. *Brain Res* **148,** 425–440.

Zimmerman CA, Leib DE & Knight ZA (2017). Neural circuits underlying thirst and fluid homeostasis. *Nat Rev Neurosci* **18,** 459.

Figure 1. Schematic model. Here, the spiking, secretion and clearance models for oxytocin cells (Maícas Royo et al. 2016; 2018), are extended to model responses to osmotic and hypovolemic stimulation. Experimentally-induced changes in osmotic pressure are mimicked by simulating the injection or infusion of i.v. or i.p. hypertonic NaCl. The resulting increases in $[Na^+]$ at the circumventricular organs result in increased afferent input to the oxytocin cells. These activate an excitatory input from the OVLT and the subfornical organ (SFO), and indirectly activate an inhibitory input from the median preoptic area (MnPO). Thus the input to oxytocin cells comprises a mixture of EPSPs and IPSPs, and the rate of that input is assumed to be linearly proportional to extracellular $[Na^+]$. When NaCl is injected i.v., it is assumed to diffuse from plasma into the EVF homogeneously at all body sites; the rate of diffusion is determined by the time constant τ_{iv} and by the concentration difference between plasma and EVF. Water moves by osmosis from the ICF to the EVF to maintain osmotic equilibrium in all compartments. By contrast when NaCl is injected i.p., it enters the peritoneal EVF; from here it enters the plasma with a diffusion time constant τ_{ip}. Thus sites distant from the peritoneum, like the circumventricular organs, receive Na^+ by diffusion from the plasma and by diffusion through the EVF. We assume here that the changes at the circumventricular organs closely mirror those in plasma. In some experiments we model hypovolemia as a stimulus that reducing plasma volume, increases the EVF volume and inhibits the inhibitory component of osmoreceptive afferent inputs.

Figure 2. **The diffusion model of Na^+.**

A) [Na^+] dynamics in plasma and EVF during a 30 min i.v. infusion of 2M NaCl at 26 µl.min^{-1}. The white dots show plasma [Na^+] from Leng *et al.* (2001). These data were fit to the model to estimate the time constant τ_{iv} of diffusion of NaCl from plasma to EVF, and the red line shows the fit of the model to the plasma [Na^+] measurements. The purple line is the inferred [Na^+] in the EVF. See Table 1 for the parameter values of the Na^+ distribution model.

B) Inferred changes in the volumes of EVF and ICF during the i.v. infusion; these are the changes necessary to maintain osmotic equilibrium between the body fluid compartments.

C) Using the same parameter values as in A and B, the model can simulate the [Na^+] dynamics after an i.p. NaCl injection, as described in Brimble & Dyball (1977).

D) The symbols show mean (SE) values of plasma osmotic pressure measured after i.p. injection of 1 ml 1.5 M NaCl; data from Brimble & Dyball (1977). The data have been converted to estimates of [Na^+] (see Methods).

E) The inferred changes in EVF and ICF volumes following i.p. injection of hypertonic saline.

Figure 3. The single neurone model.
A) The black circles show the firing rate (in 16-s bins) of a single oxytocin cell (from Leng *et al.* 2001) in response to an i.v. injection of CCK, and to an i.v. infusion of 2M NaCl at 26 µl min^{-1}. The red line shows the same experimental protocol mimicked in a model oxytocin cell. The model of Maícas Royo *et al*. (2018) was adjusted for the rat weight in this experiment and the basal PSP rate was set to match the observed mean basal firing rate (2.29 spikes s^{-1}). The CCK injection was modelled exactly as in Maícas Royo *et al*. (2018) (as a step increase in EPSP rate that decays exponentially, using parameters as in that paper).The i.v. infusion was mimicked as a linear increase in PSP rate with the slope estimated from the experiments in Figures 2 and 4.
B) The firing rate of the model neurone in 1-s bins, displaying variability similar to that observed in recorded oxytocin cells. The basal firing rate (left), is 2.29 spikes s^{-1}. After the simulated NaCl infusion, the firing rate increased by 8 spikes s^{-1} (right).
C) Predicted secretion from the model neurone during the activity shown in **B**. Because of the non-linear coupling between spike rate and secretion, the model predicts a proportionately larger increase in secretion than in firing rate.

Figure 4. Oxytocin spiking and plasma responses to changes in osmolality. We ran the model using the same parameter values as in Fig 2, adjusting just the basal firing rate, the rat's weight and the amount and origin of NaCl injected.

A) White dots show the mean (SE) firing rate of 12 oxytocin cells during i.v. infusion of 2M NaCl at 26 µl min^{-1} (from Leng *et al.*, 2001). In orange, the mean firing rate of 30 model neurones with a mean (SD) basal PSP rate I_{re} = 305(150) s^{-1} in response to simulation of the same challenge.

B) The open circles show the mean (SE) plasma oxytocin concentrations in response to the i.v. infusion as in A (from Leng *et al.*, 2001). The orange line shows the plasma concentration predicted from the model, derived from the summed predicted secretion of 100 model neurones (with basal activities randomised as in **A**), multiplied by 100 to scale to secretion from 10,000 oxytocin cells.

C) The black dots reproduce data from Brimble & Dyball (1977) and show the mean (SE) firing rates of 11 oxytocin cells in response to i.p. injection of 1 ml 1.5M NaCl. The blue line shows the results of simulating this experiment in 30 model neurones.

D) The black dots reproduce data from Higuchi *et al.* (1985), and show mean (SE) plasma oxytocin concentrations after i.v. injection of 0.38 ml 1.5M NaCl. The purple line shows the results of simulating this experiment derived as in **B** from the summed secretion of 100 model neurones multiplied by 100 to scale to secretion from 10,000 oxytocin cells, with the same parameter values as in **A**, **B** and **C**.

E) The green triangles reproduce data from Brimble & Dyball (1977), and show the relationship between firing rate and plasma osmotic pressure for 53 oxytocin cells. The black circles show the corresponding predicted values for 50 model neurones with randomised basal PSP rates (mean 170, SD 85 s^{-1}).

Figure 5. Response to bicuculline.

A) The blue triangles show the mean (SE) firing rate response of five oxytocin cells to i.v. infusion of 2M NaCl at 26 µl.min^{-1}. The red squares show the responses after blocking IPSPs by application of bicuculline to the supraoptic nucleus (from Leng *et al*., 2001).

B) The experiments in A were simulated in 20 model neurones with mean (SD) basal PSP rates of I_{re} = 210 (100) s^{-1}. The blue line shows the mean firing rate increment to the simulated infusion. The red line shows responses of model neurones when the effect of bicuculline was simulated by setting I_{ri} =0.

Figure 6. Responses to hypovolaemia.

A) After injecting rats with polyethylene glycol to induce hypovolaemia, plasma concentrations of oxytocin (black triangles) are higher than in normal rats (red squares), and the difference increases with plasma [Na^+]; data from Stricker & Verbalis (1986).
B) The orange line shows the relationship in the model between plasma oxytocin concentration and [Na^+]. The blue line shows the relationship when $I_{ri} = 0$.
C) The black line shows the effect, predicted in the model, of hypovolemia on the measured plasma concentrations of oxytocin, mimicking the conditions in **A.**
D) The predicted oxytocin concentrations in plasma (blue squares) and EVF (red squares) for a *constant* rate of secretion and different degrees of hypovolaemia.
E) Predicted total plasma content of oxytocin when the rate of secretion increases from 0 (at time 0) to a steady constant rate, in rats with simulated hypovolaemia as induced by polyethylene glycol. With large plasma volume reductions, (2 ml, green line; 3.5 ml, black line), the plasma oxytocin content takes longer to reach equilibrium than normal (red line) However, for a fixed constant secretion rate, the total amount of oxytocin in plasma is unchanged at equilibrium, so the oxytocin concentration in plasma rises in proportion to the reduced volume.
F) As **E**, but showing the predicted total oxytocin content of the EVF.
Note that the model (**B** and **C**) gives values of plasma oxytocin ~20 times higher than shown in **A** because it simulates the oxytocin levels as measured by the Higuchi immunoassay (Higuchi *et al.*, 1985). This reports higher values than the radioimmunoassay with the antibody Pitt-Ab-2 used in **A**. See the *Discussion* for a fuller account.

Table 1.

Top) Parameters of the integrate-and-fire spiking model, from Maícas Royo *et al*. (2018).

Bottom). Parameters to fit the osmotic model. In the simulations, I_{re} varied to produce different basal firing rates as appropriate; I_{ratio} was varied to simulate the experiments where IPSPs were reduced; the other parameters were unchanged from the upper table.

Name	Description	Value	Units
$\boldsymbol{I_{reBasal}}$	Basal excitatory input rate	292	$PSPs.s^{-1}$
$\boldsymbol{I_{ratio}}$	Ratio between IPSP and EPSP rates	0.75	
$\boldsymbol{e_h}$	EPSP amplitude	2	mV
$\boldsymbol{i_h}$	IPSP amplitude	-2	mV
$\boldsymbol{\lambda_{syn}}$	PSP half-life	3.5	ms
$\boldsymbol{k_{HAP}}$	HAP amplitude per spike	30	mV
$\boldsymbol{\lambda_{HAP}}$	HAP half-life	7.5	ms
$\boldsymbol{k_{AHP}}$	AHP amplitude per spike	1	mV
$\boldsymbol{\lambda_{AHP}}$	AHP half-life	350	ms
$\boldsymbol{V_{rest}}$	resting potential	-56	mV
$\boldsymbol{V_{thresh}}$	spike threshold	-50	mV
$\boldsymbol{\tau_{ip}}$	Na^+ time constant after i.p. injection	0.0006	s^{-1}
$\boldsymbol{\tau_{iv}}$	Na^+ time constant after i.v. injection	0.0036	s^{-1}
$\boldsymbol{\tau_w}$	membrane crossing time constant of water	1.61	s^{-1}

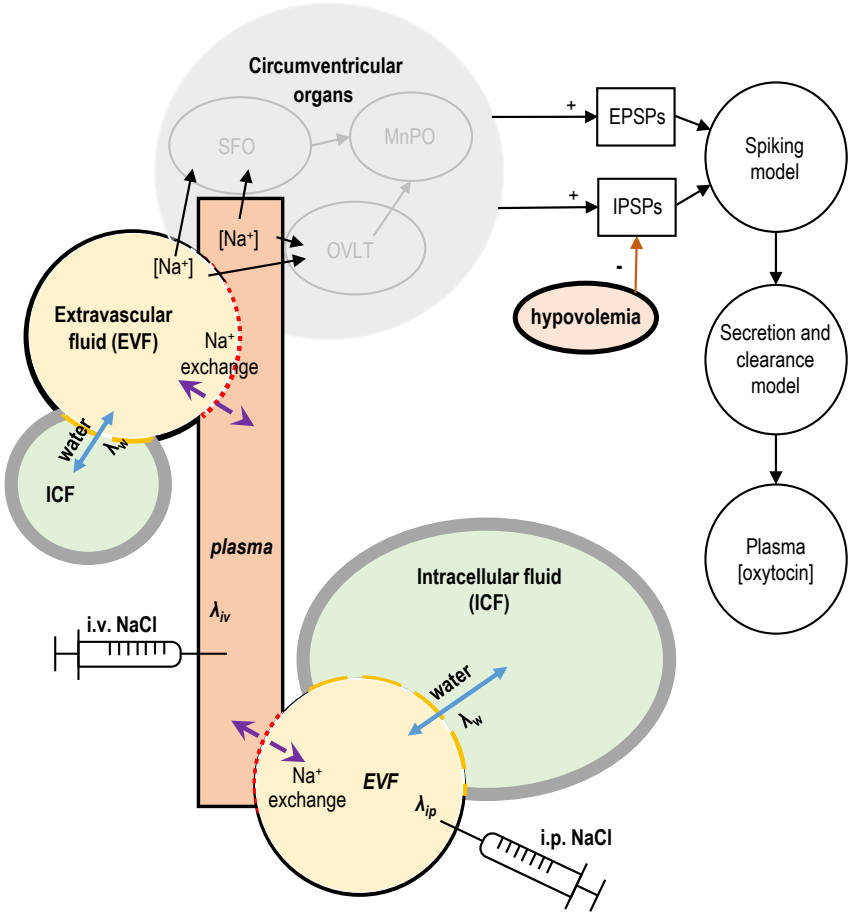
Circumventricular organs
SFO
MnPO
OVLT
[Na+]
[Na+]
+
EPSPs
+
IPSPs
-
hypovolemia
Spiking model
Secretion and clearance model
Plasma [oxytocin]
Extravascular fluid (EVF)
Na+ exchange
water
λw
ICF
plasma
λiv
i.v. NaCl
Intracellular fluid (ICF)
water
λw
Na+ exchange
EVF
λip
i.p. NaCl

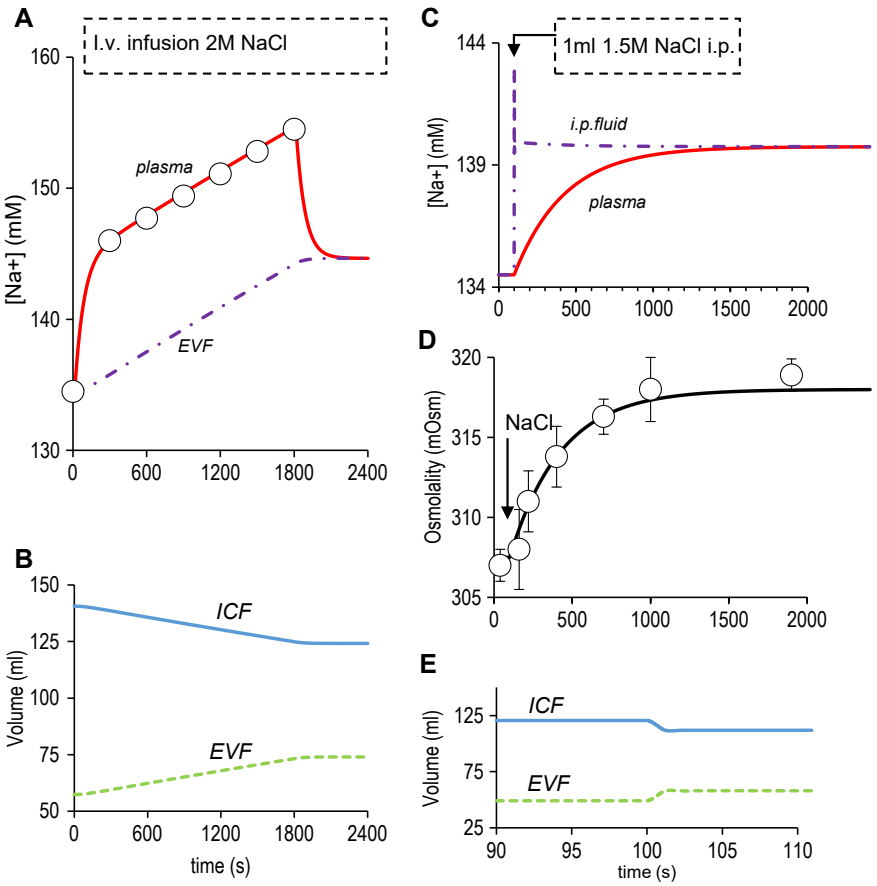
A
I.v. infusion 2M NaCl
[Na+] (mM)
160
150
140
130
plasma
EVF
0
600
1200
1800
2400
B
Volume (ml)
150
125
100
75
50
ICF
EVF
time (s)
C
1ml 1.5M NaCl i.p.
[Na+] (mM)
144
139
134
i.p.fluid
plasma
0
500
1000
1500
2000
D
Osmolality (mOsm)
320
315
310
305
NaCl
E
Volume (ml)
125
75
25
ICF
EVF
90
95
100
105
110
time (s)

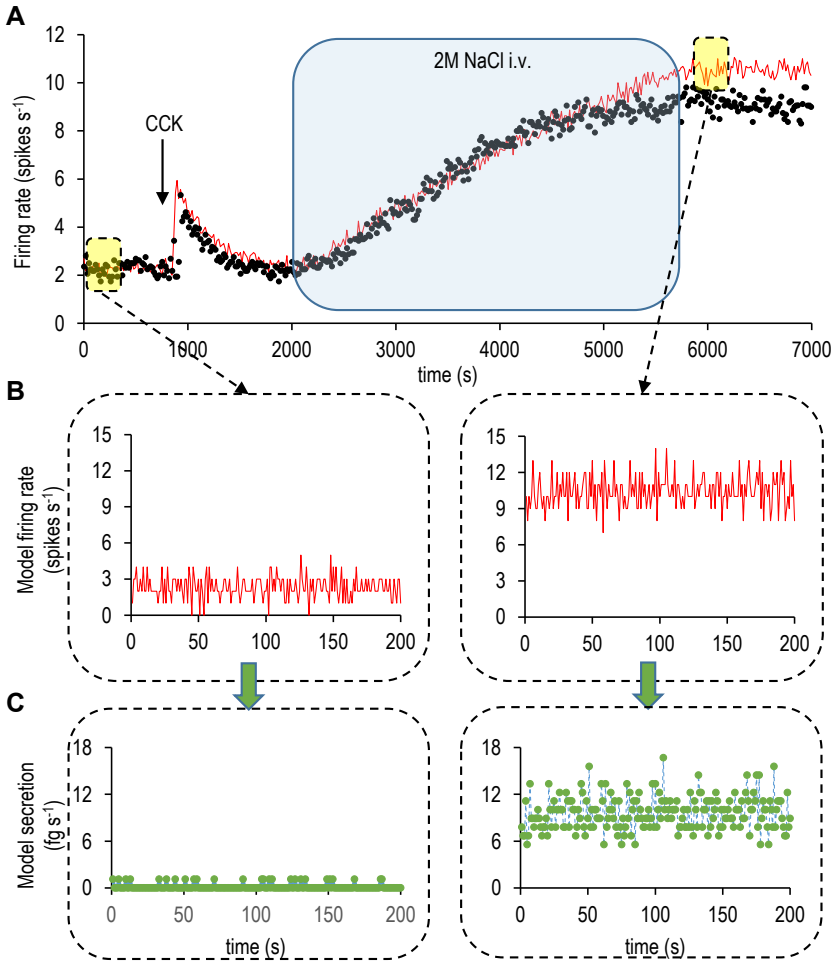
A
2M NaCl i.v.
CCK
Firing rate (spikes s-1)
time (s)
B
Model firing rate (spikes s-1)
C
Model secretion (fg s-1)
time (s)
time (s)

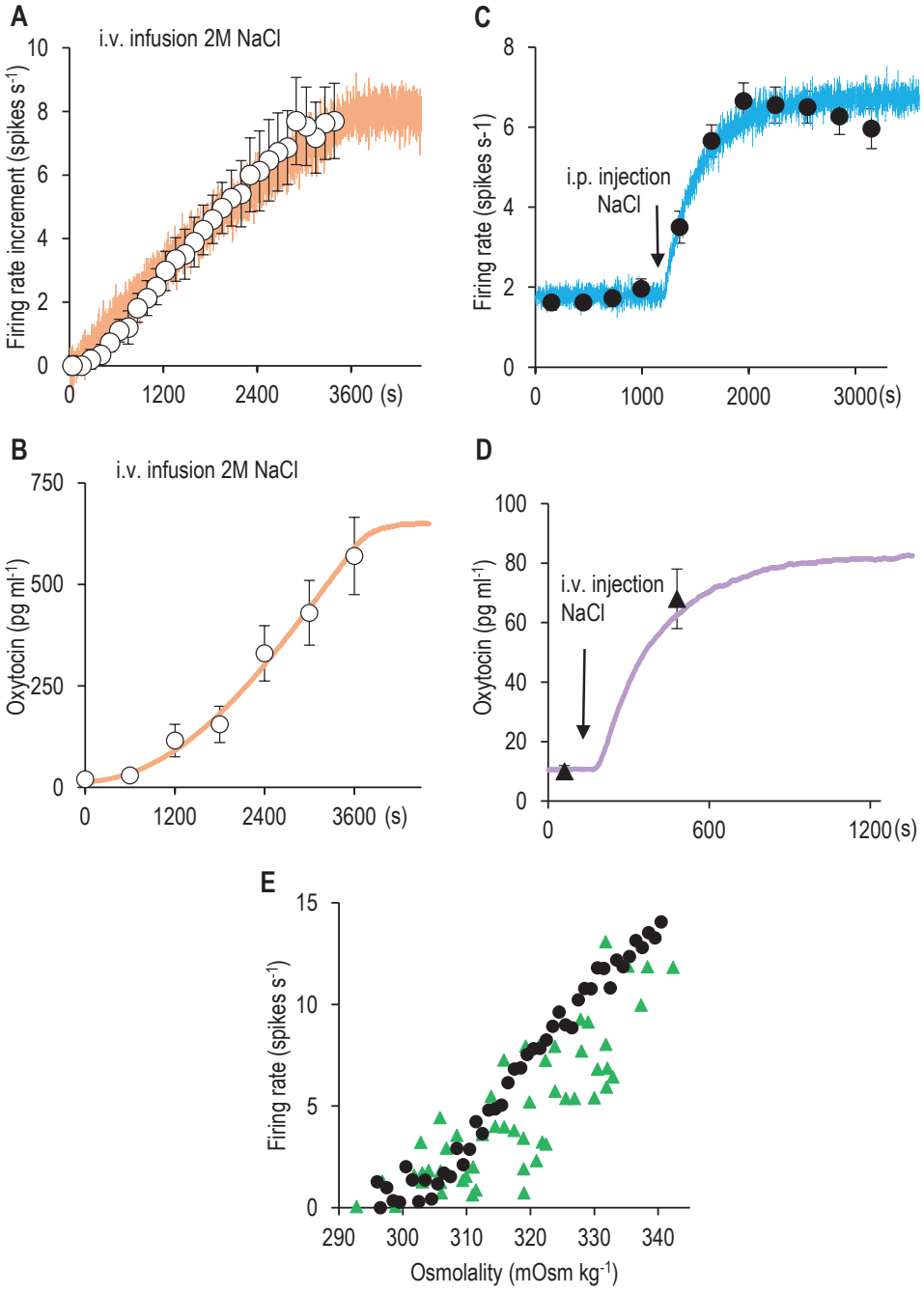
A
i.v. infusion 2M NaCl
Firing rate increment (spikes s-1)
10
8
6
4
2
0
0
1200
2400
3600 (s)
C
Firing rate (spikes s-1)
8
6
4
2
0
i.p. injection
NaCl
0
1000
2000
3000(s)
B
i.v. infusion 2M NaCl
Oxytocin (pg ml-1)
750
500
250
0
0
1200
2400
3600 (s)
D
Oxytocin (pg ml-1)
100
80
60
40
20
0
i.v. injection
NaCl
0
600
1200(s)
E
Firing rate (spikes s-1)
15
10
5
0
290
300
310
320
330
340
Osmolality (mOsm kg-1)

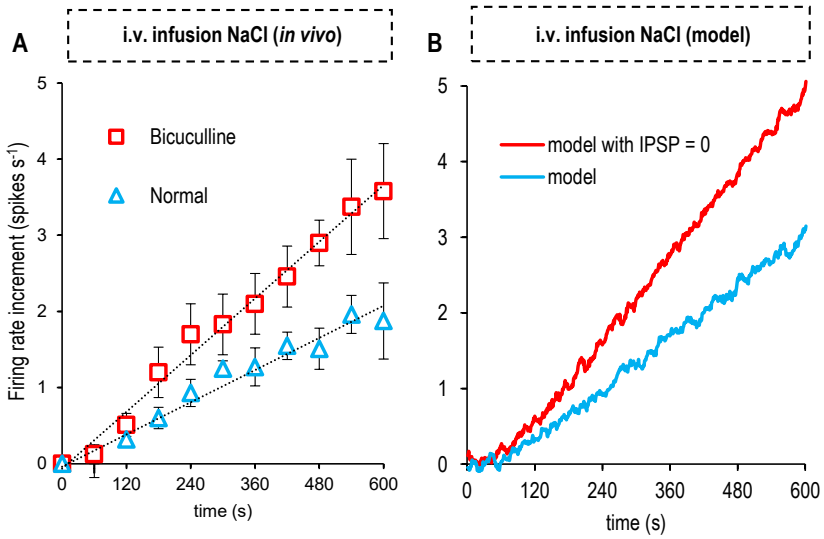
A
i.v. infusion NaCl (*in vivo*)
Bicuculline
Normal
Firing rate increment (spikes s-1)
time (s)
B
i.v. infusion NaCl (model)
model with IPSP = 0
model
time (s)

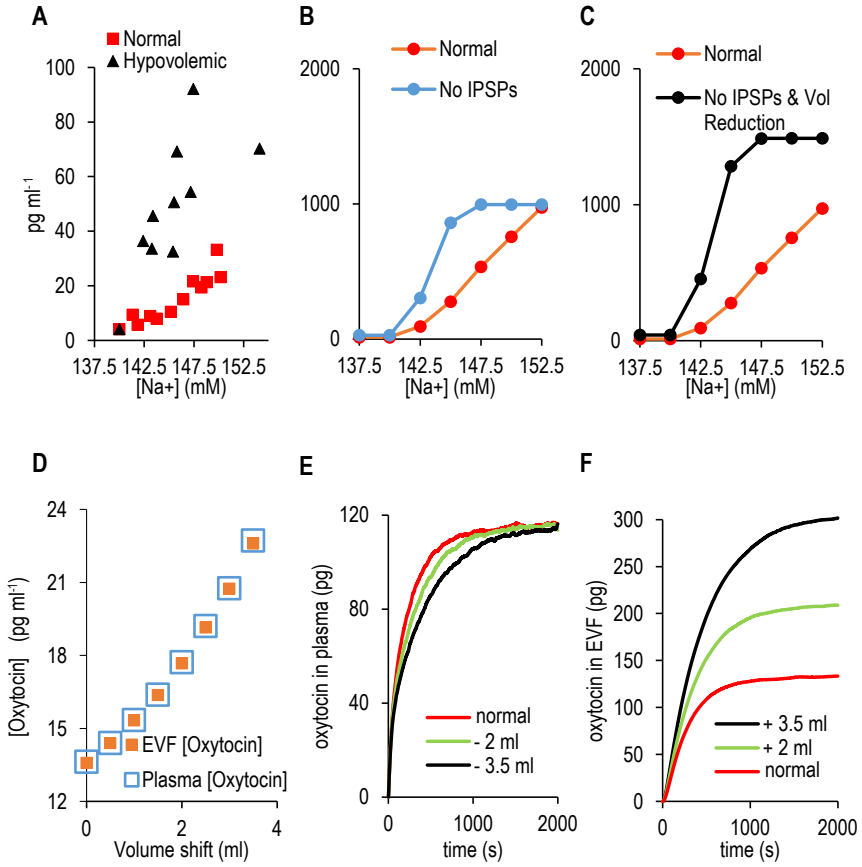
A
Normal
Hypovolemic
pg ml-1
100
80
60
40
20
0
137.5 142.5 147.5 152.5
[Na+] (mM)
B
Normal
No IPSPs
2000
1000
0
137.5 142.5 147.5 152.5
[Na+] (mM)
C
Normal
No IPSPs & Vol Reduction
2000
1000
0
137.5 142.5 147.5 152.5
[Na+] (mM)
D
[Oxytocin] (pg ml-1)
24
21
18
15
12
EVF [Oxytocin]
Plasma [Oxytocin]
0 2 4
Volume shift (ml)
E
oxytocin in plasma (pg)
120
80
40
0
normal
- 2 ml
- 3.5 ml
0 1000 2000
time (s)
F
oxytocin in EVF (pg)
300
250
200
150
100
50
0
+ 3.5 ml
+ 2 ml
normal
0 1000 2000
time (s)